Research Article | Vol. 12, No. 7 / 1 July 2021 / Biomedical Optics Express 4423
Biomedical Optics EXPRESS

Endoscopic ultrasound (EUS)-guided cylindrical interstitial laser ablation (CILA) on *in vivo* porcine pancreas

VAN GIA TRUONG,[1,5] SEOK JEONG,[2,5] JIN-SEOK PARK,[2] VAN NAM TRAN,[1] SUNG MIN KIM,[3] DON HAENG LEE,[2] AND HYUN WOOK KANG[1,4,*]

[1]*Industry 4.0 Convergence Bionics Engineering, Pukyong National University, Busan, Republic of Korea*
[2]*Department of Internal Medicine, Inha University School of Medicine, and the National Center of Efficacy Evaluation for the Development of Health Products Targeting Digestive Disorders, Inha University Hospital, Incheon, Republic of Korea*
[3]*Bluecore Company, Inc., Busan, Republic of Korea*
[4]*Department of Biomedical Engineering, Pukyong National University, Busan, Republic of Korea*
[5]*These authors contributed equally to this work*
[*]*wkang@pukyong.ac.kr*

Abstract: This study aims to demonstrate the feasibility of cylindrical interstitial laser ablation (CILA) in porcine pancreatic tissue to develop a EUS-guided PC ablation technique with enhanced safety. A diffusing applicator created a uniformly symmetrical laser ablation in pancreatic tissue. *Ex vivo* tests presented that both ablation thickness and volume increased linearly with the applied power ($R^2 = 0.96$ and 0.90, respectively) without carbonization and fiber degradation. The numerical simulations matched well with the experimental results in terms of temperature development and thermal damage (deviation of ≤ 15%). *In vivo* tests with EUS confirmed easy insertion and high durability of the diffusing applicator. EUS-guided CILA warranted a feasible therapeutic capacity of ablating *in vivo* pancreatic tissue. The proposed EUS-guided CILA can be a feasible therapeutic approach to treat PC with predictable thermal ablation and enhanced safety.

1. Introduction

Pancreatic adenocarcinoma (PC) is one of the most common cancers in the United States that develops proliferative stroma in the exocrine cells. PC is accountable for more than 8% of the annual mortality rate in the United States [1]. Although the actual survival has improved over the past decades, the 5-year survival rates are still below 5% in all stages of PC [1, 2]. Recently, endoscopic ultrasound (EUS)-guided ablation has evolved as a potentially safe and effective treatment option for an unresectable pancreatic tumor (tumor size less than 3 cm) owing to real-time imaging and focal ablation [3–6]. A variety of ablative thermal techniques have been developed to directly treat local pancreatic tumors, such as high intensity focused ultrasound (HIFU), radiofrequency ablation (RFA), and interstitial laser ablation (ILA) [4–7]. Despite the therapeutic advantage of non-invasiveness, HIFU often suffers from low treatment precision because of the obstruction of acoustic energy by interpositions (bowel gas), leading to thermal injury to the skin and incomplete ablation of target tissue [8, 9]. Although RFA in conjunction with EUS is a clinically well-accepted treatment for the unresectable pancreatic tumor, direct contact of an electrode with the tissue is associated with the contact-associated risk, such as tissue adhesion or tissue charring [5, 9, 10]. In fact, because of small ablation volume (0.24 ± 0.08 cm^3) generated by a single electrode, RFA often requires multiple treatments to cover the entire tumor size (2~5 cm^3) in clinical situations, thus increasing the risk of procedural complications,

#427379 https://doi.org/10.1364/BOE.427379
Journal © 2021 Received 16 Apr 2021; revised 5 Jun 2021; accepted 8 Jun 2021; published 24 Jun 2021

Biomedical Optics EXPRESS

including bleeding and mechanical trauma [9–11]. Di Matteo *et al.* demonstrated the feasibility of US-guided ILA as a minimally invasive treatment to achieve localized coagulation necrosis in *ex vivo* pancreatic tissue and human PC in the first clinical study [6, 12, 13]. Despite the promising results, ILA with an end-firing flat fiber generated significant carbonization in the tissue because of the small beam size (300 μm in diameter). Both high irradiance (i.e. power density; W/cm^2) and large beam divergence from the flat fiber cause excessive heating and carbonization at the fiber tip, peripheral thermal injury, non-uniform treatment volume, and fiber degradation from the tissue carbonization [12–14].

For decades, laser fibers with diffusing applicators have been developed and used for clinical situations such as photodynamic therapy (PDT) and laser interstitial thermal therapy (LITT) on various tumors (brain, breast, and liver) [15–17]. However, these availabilities on the market still remain limitations, such as non-uniform light irradiation and a narrow range of powers and wavelengths, which may cause unpredictable therapeutic outcomes and less flexibility. Contrary to available diffusing fibers for laser application, we introduce a diffusing applicator to produce a circumferential light distribution as well as deliver a wide range of powers (up to 100 W) and wavelengths (400 ~ 2200 nm). The diffusing applicator generates radial light emissions along the fiber tip and creates a layer of cylindrical ablation in the tissue. Unlike the flat fiber, the diffusing applicator has a low irradiance (i.e., power density) from a constant and wide light diffusion that can rapidly ablate a large surface area of the tissue without excessive heating and tissue carbonization [18, 19]. Thus, the application of 1064-nm Nd:YAG laser light through the

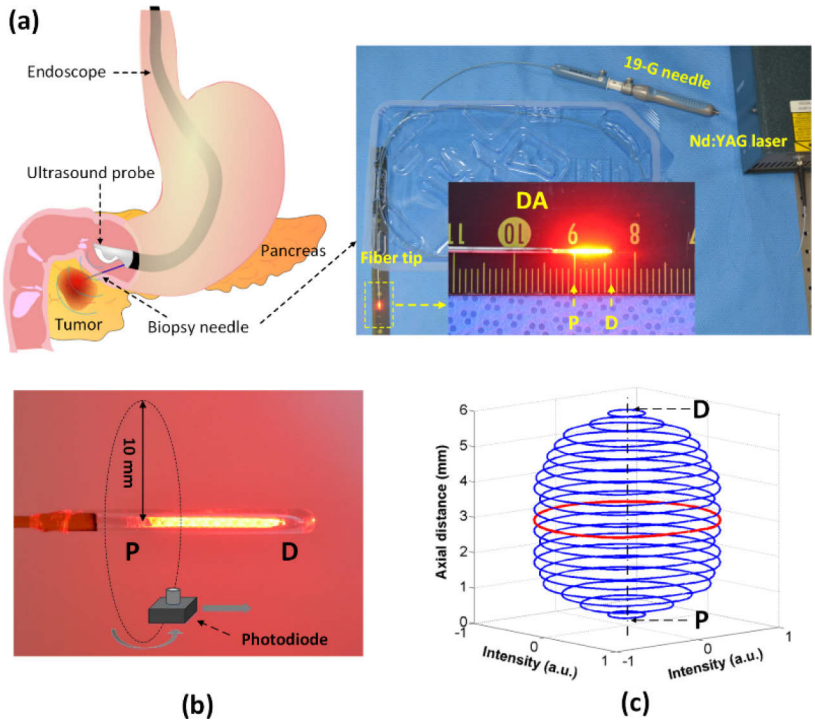

Fig. 1. Circumferential interstitial laser ablation (CILA) of pancreatic tissue: (a) illustration of endoscopic ultrasound (EUS)-guided CILA on pancreatic adenocarcinoma with diffusing applicator through small biopsy needle (19-G), (b) uniform HeNe light distribution along diffusing applicator (P = proximal and D = distal ends), and (c) 3D normalized spatial emission profile measured by photodiode in (b). Red color represents the polar intensity measured 3 mm away from P (normalized polar intensity = 0.9 ± 0.1).

Biomedical Optics EXPRESS

diffusing applicator can achieve a predictable and desirable ablation volume with a deep and wide penetration of the light into the tissue [9, 20]. The current study aims to demonstrate the feasibility of cylindrical interstitial laser ablation (CILA) in *ex vivo* and *in vivo* porcine pancreatic tissue to develop an EUS-guided laser ablation of PC with enhanced safety (Fig. 1(a)). We hypothesize that the diffusing applicator with the cylindrical light emissions induces radial heat conduction, leading to a predictable ablation volume in the pancreatic tissue with no or minimal thermal injury and carbonization. It should be noted that CILA is associated with a thermal coagulative regime, similar to other techniques [9, 21]. Using numerical simulations and both *ex vivo* and *in vivo* validations, we characterize the ablative performance of the proposed CILA technique in light of spatiotemporal developments of temperature, the extent of coagulation necrosis, and the histological response in the pancreatic tissue.

2. Materials and methods

2.1. Fiber preparation

A diffusing applicator (active length = 6 mm and core fiber diameter = 400 μm; Tecure, Inc., Busan, South Korea) was used to emit laser light in a circumferential direction (Fig. 1(b)). The detailed fabrication were presented in the previous study [20]. The micro-machined surface of the fiber tip allowed for a partial internal reflection inside the fiber for radial light diffusion. A customized glass cap (i.e., length = 8 mm, inner diameter = 0.5 mm, and outer diameter = 0.7 mm) was glued to the fabricated tip by using epoxy to prevent any mechanical damage. HeNe light (λ = 632 nm, Thorlabs Inc., Newton, New Jersey, USA) visually confirmed the uniform light distribution along the diffusing tip (Fig. 1(b)). A goniometer and photodiode (PD-300-3W, Ophir, Jerusalem, Israel) were used to measure the light intensity exiting the fiber and diffusing applicator to evaluate the diffusing performance [20]. The total light transmission from the diffusing tip was 95%, and the normalized longitudinal intensity was estimated to be 0.89 ± 0.12 a.u. (arbitrary units). The polar emissions had an almost isotropic radiation with less than 10% deviation, indicating a homogenous and cylindrical light distribution from the diffusing applicator (Fig. 1(c)).

2.2. Numerical simulations

Numerical simulations were performed to predict the thermal effects of CILA applications on porcine pancreatic tissue under various conditions. The numerical simulations helped to determine the optimal treatment conditions by showing the spatiotemporal developments of the temperature field (Fig. 2(a)) and the extent of thermal denaturation (Fig. 2(b)). A partial differential equation was solved by using COMSOL Multiphysics software (v5.3, COMSOL Inc., Burlington, Massachusetts). Based upon physical dimensions of a diffusing applicator and the experimental setups, simulation models for single CILA used two geometries for quantitative evaluations on temperature profile (Fig. 2(a)) and thermal damage (Fig. 2(b)). The tissue was constructed in a size of 30×30×30 mm^3. A single diffusing applicator (core diameter = 400 μm; active length = 6 mm; glass cap length = 8 mm; outer diameter = 0.7 mm) was placed on the tissue surface (Fig. 2(a)) or inserted into the tissue (Fig. 2(b)). A 1064 nm wavelength was employed to irradiate laser light into the tissue for the current study. All conditions were employed in simulation model following the experimental setups. Table 1 summarizes physical and optical properties of pancreatic porcine tissue used in the current simulations. Due to lack of data, all the properties were assumed to be constant for the simulations.

The Pennes bioheat transfer equation was incorporated with the Beer's law to describe heat transfer in the tissue during laser irradiation, which is described as follows [21, 22]:

$$\rho c \frac{\partial T(r,z,t)}{\partial t} = \nabla \cdot (k \nabla T(r,z,t)) + \rho_b c_b \omega_b (T_b - T(r,z,t)) + Q_{met} + Q_{eva} + Q_{ext} \quad (1)$$

Biomedical Optics EXPRESS

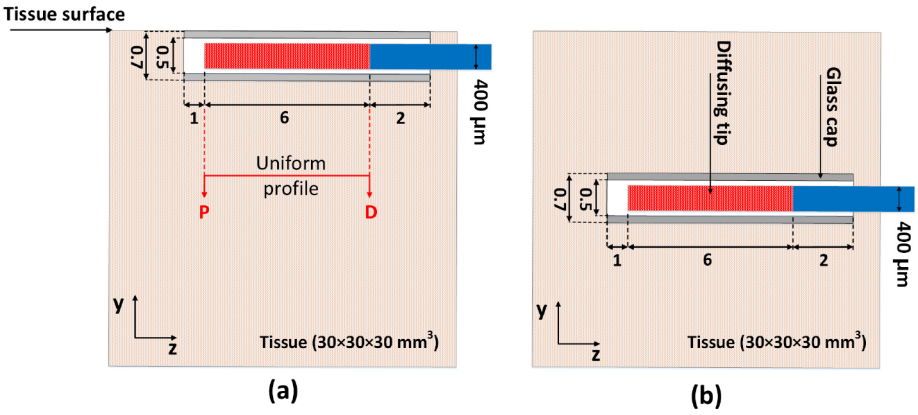

Fig. 2. Schematic illustrations of geometries for numerical simulations on (a) temperature evaluation and (b) extent of coagulation lesion (P = proximal and D = distal ends of diffusing tip). Note that a diffusing applicator in (a) is placed on the tissue surface whereas a diffusing applicator in (b) is embedded inside the tissue; scale in mm.

Table 1. Summary of physical and parameters used in numerical simulations[a]

Parameter	Value	Unit	References
Absorption coefficient (μ_a)	0.9 ± 0.1	cm^{-1}	[25]
Scattering coefficient (μ_s)	130 ± 1	cm^{-1}	[25]
Anisotropy factor (g)	0.82 ± 0.01		[25]
Density (k)	0.51	$W/(m.K)$	[26]
Specific heat (c)	3164	$J(kg.K)$	[26]
Thermal conductivity (p)	1045	kg/m^3	[26]
Frequency factor (A_f)	3.1×10^{98}	$1/s$	[21]
Activation energy (E_a)	6.28×10^5	J/mol	[21]
Universal gas constant (R)	8.314	$J/(mol.K)$	[21]

[a]Critical temperature for irreversible thermal coagulation; $T_{crit} = E_a/R \ln\{A_f\} \approx 60°C$

where ρ (kg/m^3), c (J/kg·K), and k (W/m·K) are density, specific heat, and thermal conductivity of the pancreatic tissue, respectively, T(r,z,t) is the tissue temperature. For blood parameters, ρ_b (kg/m^3), c_b ($J/kg{\cdot}K$), ω_b (s^{-1}), and T_b (310 K) are density, specific heat, blood perfusion rate per unit volume in tissue, and the temperature of arterial blood, respectively. Q_{met} (W/m^3) denotes the metabolic heat generation per unit volume through the oxidative process. No blood perfusion and no metabolic heat generation were considered in the numerical simulations. Other terms are defined below:

- Q_{eva} (W/m^3) is the energy density due to water evaporation (i.e., ≥ 100 °C), which can be expressed by [22]:

$$Q_{eva} = -h_{fg} \cdot \frac{d\rho_w}{dt} \tag{2}$$

where h_{fg} (J/kg) indicates the latent heat for water evaporation and ρ_w denotes water density (kg/m^3) as a function of temperature. At 100 °C, water evaporation happens to cause the change of heat capacity, necrosis, and the loss of cellular physiological activity [23]. Thus,

Biomedical Optics EXPRESS

the parameter ρ_w can be expressed as follows [22]:

$$\rho_w(T) = 0.778 \times \begin{cases} 1 - e^{(T-106)/3.42} & T \le 103°C \\ 0.03713T^3 - 11.47T^2 + 1182T - 40582 & 103°C<T<104°C \\ e^{(T-80)/34.37} & T \ge 104°C \end{cases} \tag{3}$$

• Q_{ext} (W/m^3) represents the external heat source in the radial direction, following the Beer-Lambert law:

$$Q_{ext} = \mu_a \cdot \frac{P}{2\pi rl} \exp(-\sqrt{3\mu_a(\mu_a + \mu_s(1-g))} \cdot r) \tag{4}$$

where μ_a (cm^{-1}) is the absorption coefficient of laser light in tissue, μ_s (cm^{-1}) the scattering coefficient of laser light in tissue, g the anisotropy coefficient, P (W) laser power in various power levels, r (m) the radial distance from the glass cap, and l (m) the diffusing applicator length.

The initial tissue temperature was set to 20 °C, and the external tissue surface was insulated (i.e., $\vec{n} \cdot k\nabla T = 0$). For the model of temperature evaluation in Fig. 2(a), surface convective heat loss was considered as a boundary condition at the tissue surface due to cooling effect by natural convection, and a convective coefficient was taken as 10 W/m^2·K [21, 24].

The extent of thermal damage in tissue due to the temperature dependence of molecular reaction rates was described by an Arrhenius equation (Ω) as below [21]:

$$\Omega(\mathrm{r,t}) = \mathrm{A}_f \int_0^{\tau} \exp\left(\frac{-E_a}{R.T(\mathrm{r,t})}\right) dt \tag{5}$$

where A_f $(1/s)$ is the frequency factor, E_a (J/mol) is the denaturation activation energy, R is the universal gas constant of 8.314 $(J/mol{\cdot}K)$, and τ (s) is the irradiation time. The Arrhenius equation determined the extent of thermal damage in tissue as a function of temperature and time and estimated the final ablation (ellipsoidal) volume by using the formula $\pi/6{\cdot}a{\cdot}b{\cdot}c$, where a, b, and c are the length, height, and width of the ellipsoid. $\Omega = 1$ (i.e., $\log(\Omega) = 0$) represents the irreversible thermal denaturation corresponding to the critical temperature (~ 60 °C) in tissue [21]. The numerical results were compared to experimental data to validate the thermal and histological responses of the pancreatic tissue to CILA.

2.3. Ex vivo CILA tests

Because of deep optical penetration, a 1064 nm Nd:YAG laser system (FC-W-1065, CNI, Changchun, China) was employed for the current ablation testing to evaluate temperature profiles (Fig. 3(a)) and the extent of coagulation lesion (Fig. 3(b)). The two ex vivo models used the same ablation conditions. The applied power levels were 3, 5, 7, 10, 15, and 20 W. For direct comparison, a total energy of 1000 J was delivered in a continuous wave mode under each power condition. The corresponding irradiation times were 333, 200, 143, 100, 67, and 50 s, respectively. A local slaughterhouse supplied porcine pancreatic tissue. The pancreatic tissue samples were cut into 30×30×30 mm^3 sections and stored at 4 °C to minimize any dehydration and structural deformation. The initial tissue temperature was maintained at 20 °C.

For temperature evaluation, a 1-mm diameter biopsy needle (Disposable biopsy punch, Kai Medical, Seki City, Japan) was used to create a pattern on the sample surface in a 1-mm groove depth. Then, a diffusing applicator was carefully placed into the created pattern of each specimen (Fig. 3(a)). An infrared (IR) thermal camera (320×240 pixels, 15 Hz acquisition rate, FLIR A310, Inc., Oregon, USA) was positioned 40 cm above the sample surface to record spatiotemporal

Biomedical Optics EXPRESS

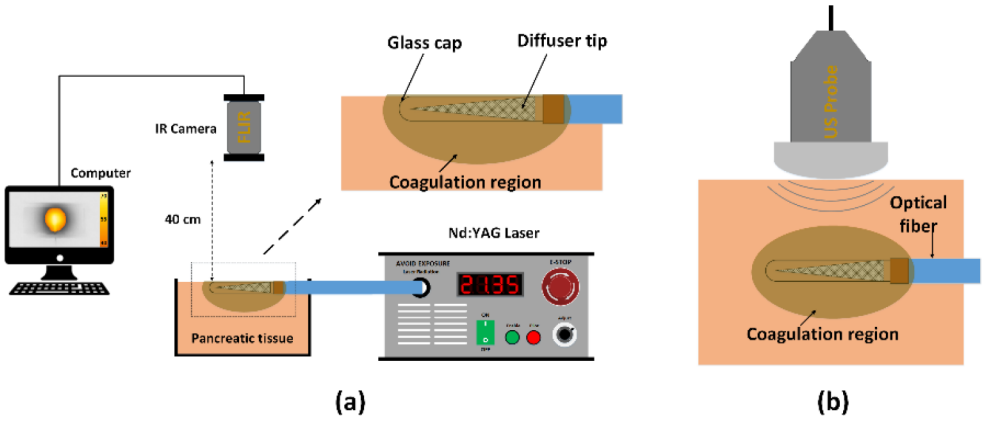

Fig. 3. Experimental setups for (a) temperature evaluation (N = 5) and (b) US monitoring (N = 10) during laser ablation of porcine pancreatic tissue at various conditions. Note that a diffusing applicator in (a) is placed on the tissue surface whereas a diffusing applicator in (b) is embedded inside the tissue.

developments of surface temperature as well as temperature distribution along the diffusing applicator during irradiation. Each condition was repeated five times (N = 5).

In an attempt to evaluate the extent of coagulation volume, CILA was performed on the prepared tissue samples (Fig. 3(b)). Before ablation tests, each prepared specimen was placed in a tissue holder, which was printed by using a 3D printer (Replicator Z18^{TM}, Makerbot, New York, USA). For fiber insertion, a 1.5-mm hole was created on the side of the tissue holder. A 19-G biopsy needle (Cook Medical Inc., Indiana, US) was initially inserted into the pancreatic sample to simulate the clinical procedures of EUS-guided ablation. Then, a diffusing applicator was inserted through the needle to transmit laser light cylindrically for interstitial thermal treatment [12, 13]. A US system (UGEO HM70A, Samsung Medison Co., Ltd, Seoul, South Korea) with a 4-7 MHz probe (L4-7) helped precisely guide the insertion of both the needle and diffusing applicator into the tissue. Each condition was repeated ten times (N = 10).

2.4. *In vivo CILAs test*

Two mini-pigs (30~35 kg) were used for *in vivo* EUS-guided CLIA tests. Before the tests, all the animals were prepared for general anesthesia with an intramuscular injection of 0.04 mg/kg atropine sulfate, 2 mg/kg xylazine, and 5 mg/kg tiletamine-zonelazepam. A ventilator was used to provide isoflurane (0.5-2%) and oxygen (2 L/min) through intubation to maintain the general anesthesia. A GF-UCT260 linear-array echo endoscope (Olympus Medical Co. Ltd., Tokyo, Japan) were employed with a EU-ME2 ultrasound system (Olympus Medical Co. Ltd., Tokyo, Japan) for the EUS-guided CILA in the porcine models. Under the EUS-guidance, a 19-gauge needle was inserted into the endoscope, punctured through the stomach to reach the body of the pancreatic tissue, and withdrawn 10 mm from the endoscope. Then, a diffusing applicator was inserted into the needle catheter to transmit laser energy for ablation after reaching the tissue (see Visualization 1) [6, 12]. Based on *ex vivo* results, the *in vivo* EUS-guided CILA applied treatment conditions of 5 W and 200 s (1000 J delivered) by using a 1064 nm Nd:YAG laser system. Three hours after the ablation tests, the animals were euthanized by intravenous injection of 100 mg/kg pentobarbital for post-experimental analysis. All the animal experiments were conducted in accordance with the guidelines of the Korean National Institutes of Health (KNIH). The protocol was approved by the Institutional Animal Care and Use Committee at KNOTUS, South Korea (Permit Number: 20-KE-496).

Biomedical Optics EXPRESS

2.5. Quantification

Due to inherent nature (soft and flexible) of porcine pancreas, all treated samples were frozen at -80 °C for four hours after *ex vivo* ablation tests. Then, the frozen samples were transversely sectioned into 1-mm thick slices along the diffusing axis (six slices per sample). A digital camera (D5100, Nikon Corp., Tokyo, Japan) was used to photograph all the slices. For pathologic analysis, the treated samples from both *ex vivo* and *in vivo* tests were fixed in 10% formalin for a week. Then, the fixed samples were sectioned by 6-μm and prepared in histology slides. All the prepared slides were stained with hematoxylin and eosin (HE) and scanned by using a scanning microscope (MoticEasyCan Pro, Motic Asia Corp., Kwoloon, HongKong). Image J (National Institute of the Heath, Bethesda, MD) was used to measure the physical dimensions (radial thickness and area) of the ablated tissue (shown as discolored region). In order to estimate the degree of ablation symmetry, eccentricity was calculated by dividing the standard deviation of the radial ablation thickness by its mean value. The eccentricity of less than 15% represents the circularity of thermal ablation in tissue (transverse plane) generated by the diffusing applicator [18]. The entire ablation volume was estimated by integrating a series of the measured ablation areas with respect to the slice thickness (i.e., volume = $\int$ A(x) dx, where A(x) = measured ablation area and dx = thickness of slice).

2.6. Statistical analysis

All the data are represented as mean ± standard deviation. For statistical analysis, an ANOVA test was performed among the groups using SPSS software (SPSS Inc., Chicago, USA), and $p < 0.05$ was considered statistically significant.

3. Results

We analyzed the thermal response of *ex vivo* pancreatic tissue to CILA at various power levels, and a diffusing applicator delivered 1000 J at each power level (Fig. 4; data acquired from Fig. 3(a)). Numerical simulation exhibited an axisymmetric and elliptical distribution of the interstitial tissue temperature around the diffusing applicator after irradiation of 5 W for 200 s (left; Fig 4(a)). The highest temperature occurred at the center of the applicator. An IR image validated an elliptical shape of the temperature distribution around the diffusing applicator in the pancreatic tissue after 5-W CILA for 200 s (right; Fig. 4(a)). A measured point (MP; 1 mm away from diffusing applicator) showed that the interstitial tissue temperature increased with irradiation time, irrespective of power level (left; Fig 4(b)). The maximum tissue temperature at MP increased with the applied power (right; Fig. 4(b)). Both numerical results and experimental data showed a good agreement in the temperature developments in the pancreatic tissue during CILA. With the application of 5 W, the tissue reached the maximum temperature of 65 °C, which corresponds to the threshold temperature of coagulation necrosis in tissue (blue dashed lines; right in Fig. 4(b)). Thus, we confirmed that power levels of 5 W or higher were required to reliably achieve sizeable ablation volumes in the pancreatic tissue. Figure 4(c) presents a compilation of US images that showed the cross-sectional areas of the pancreatic tissue at various irradiation times during 5-W CILA. The US image at 0 s (left) initially identifies the position of the diffusing applicator inside the tissue. Upon irradiation, irreversible tissue ablation started to form around the diffusing applicator circumferentially. Yellow dotted lines (right image) represent changes in tissue elasticity caused by coagulation necrosis (CN; whitish region).

We examined the extent of coagulation necrosis in *ex vivo* pancreatic tissue after CILA at various power levels (equivalent energy delivery = 1000 J; data acquired from Fig. 3(b)). Numerical simulation showed that a circular shape of irreversible tissue ablation forms around the diffusing applicator after irradiation of 5 W for 200 s (left; Fig. 5(a)). A white dotted line with $\log(\Omega) = 0$ represents the boundary where coagulation necrosis is generated in the tissue.

Biomedical Optics EXPRESS

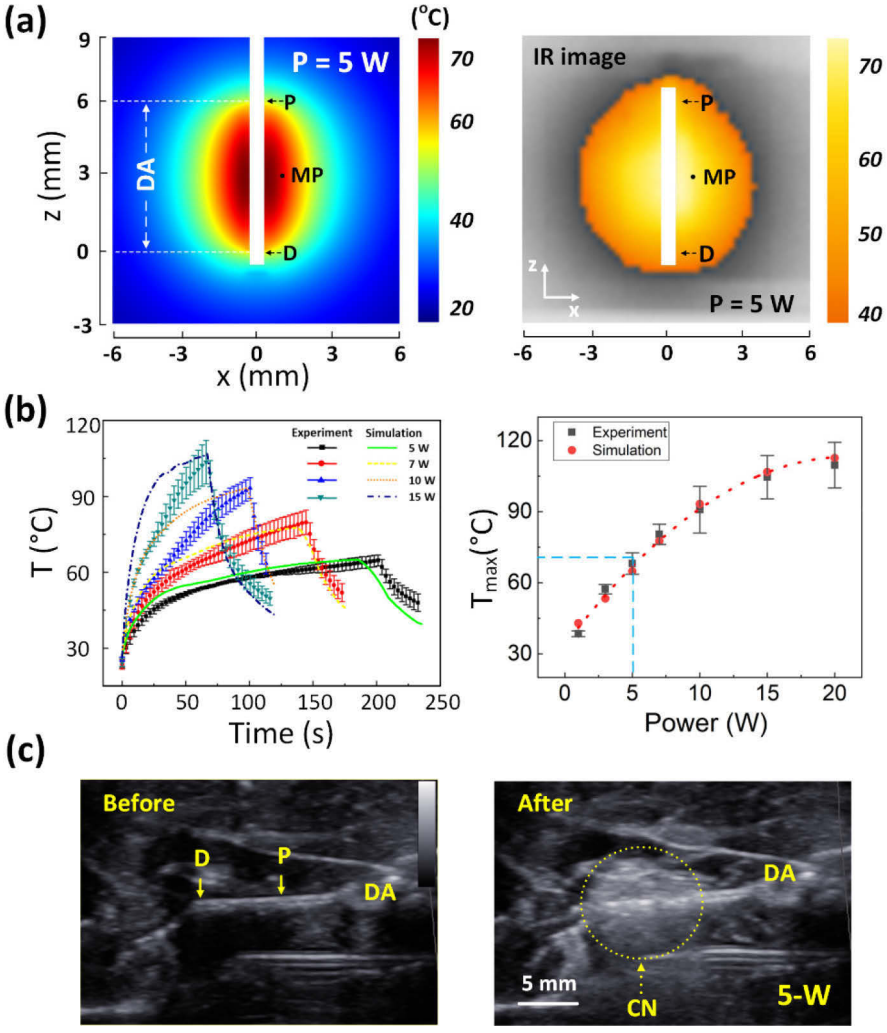

Fig. 4. Quantitative evaluations on thermal responses of ex vivo pancreatic tissue to CILA at various power levels: (a) numerical simulation (left) and experiment (right; IR image) on spatial distribution of tissue temperature after irradiation of 5 W for 200 s (1000 J delivered; DA = diffusing applicator; MP = measured point at r = 1 mm away from DA; P and D = proximal and distal ends of DA), (b) temporal developments of temperature measured at MP during 200-s irradiation at various power levels (left; 5, 7, 10, and 15 W) and maximum interstitial temperature (T_{max}) measured at MP as function of power (right; N = 5), and (c) cross-sectional US images of pancreatic tissue captured before (right) and after (left) 5-W CILA for 200 s (CN = coagulation necrosis).

Biomedical Optics EXPRESS

Correspondingly, experimental data validated the circular shape of thermal ablation from the cross-section of the tissue (zx plane) after CILA at 5 W (right; Fig. 5(a)). Figure 5(b) displays a HE-stained histology image of the transversely sectioned tissue (xy plane) that was acquired from the middle point of the diffusing tip after 5-W CILA for 200 s. Coagulation necrosis (pinkish color) was vividly observed in a circular shape (40×), indicating uniform ablation during CILA because of cylindrical light emissions from the diffusing applicator. A higher magnification image (400×) shows the well-demarcated margin between coagulated and native tissues. The coagulated zone involved a loss of cellular integrity, while no cellular deformation confirmed native pancreatic tissue. No carbonization was visually observed. The small hole at the center represents where the diffusing applicator was inserted vertically. According to numerical simulations and experimental validations, ablation thickness in a radial direction increased linearly up to 8.5 mm with the applied power ($R^2 = 0.96$; left in Fig. 5(c)). Regardless of power level, the estimated eccentricity was less than 15% (red area; left in Fig. 5(c)), indicating that CILA created a uniformly circular distribution of coagulation necrosis in the pancreatic tissue. Both numerical results and experimental data demonstrated a linear relationship between applied power and ablation volume ($R^2 = 0.90$; right in Fig. 5(c)). Thus, based on the desired ablation volume, the appropriate power level can be selected from the dosimetry findings. Table 2 summarizes *ex vivo* tissue ablation after CILA at various power levels.

Table 2. Summary of CILA at various power levels in ex vivo models (energy = 1000 J; N = 10)

Power (W)	Time (s)	Ablation thickness (mm) [range]	Ablation volume (cm^3) [range]
3	333	3.7 ± 0.7 [3.0~4.3]	0.28 ± 0.10 [0.18~0.41]
5	200	5.1 ± 0.5 [4.6~5.7]	0.65 ± 0.19 [0.48~0.91]
7	143	5.6 ± 0.4 [5.0~6.2]	0.86 ± 0.19 [0.60~1.18]
10	100	6.5 ± 0.7 [5.4~7.6]	1.38 ± 0.29 [0.83~1.77]
15	67	7.7 ± 0.7 [6.7~8.3]	2.04 ± 0.39 [1.43~2.43]
20	50	8.4 ± 0.6 [7.5~8.7]	2.84 ± 0.53 [2.06~3.14]

To evaluate the feasibility of EUS-guided CILA for clinical situations, mini-pig models were tested with 5-W 1064 nm laser light for 200-s irradiation (1000 J delivered; Fig. 6). A diffusing applicator was smoothly inserted into a 19-G needle without any bending or physical damage. During laser irradiation, the applicator maintained its structural integrity to generate uniform ablation in the pancreatic tissue (see Visualization 2). Figure 6(a) shows the captured EUS images before and after 5-W CILA. The EUS image (left; Fig. 6(a)) clearly visualized the position of the applicator tip inside the pancreatic tissue (yellow arrowheads). After the irradiation, the EUS image revealed a hyperechoic area along of the diffusing tip that represented the formation of uniform coagulation necrosis (red arrows) resulting from 5-W CILA (right; Fig. 6(a)). Figure 6(b) shows two HE-stained histology images (40×) of the ablated tissue transversely acquired from two different positions after CILA: middle (A-Á) and distal end (B-B´) of diffusing applicator (inlet; right in Fig. 6(a)). Regardless of position, the EUS-guided CILA created a uniformly circular shape of coagulation necrosis around the diffusing applicator. A higher magnification image (100×; inlet; left in Fig. 6(b)) demonstrates microscopic details of the concentric nonviable coagulation necrosis (CN; complete denaturation), partially viable hyperemic transition zone (TZ; partial denaturation), and viable normal tissue (NT) in the treated tissue. CN clearly involved a loss of cellular integrity due to enzyme denaturation, while no cellular deformation was confirmed in NT. TZ verified the presence of granulocytes and histiocytes, indicating partial viability and enzyme denaturation. No carbonization was visually observed around the diffusing applicator. The distal end accompanied a moderate reduction in coagulation necrosis because of an elliptical distribution of the tissue temperature (Fig. 4(a)), which agrees well with a previous study [20]. The maximum ablation thickness measured from the *in vivo* tests (5.2 ± 0.7 mm)

Biomedical Optics EXPRESS

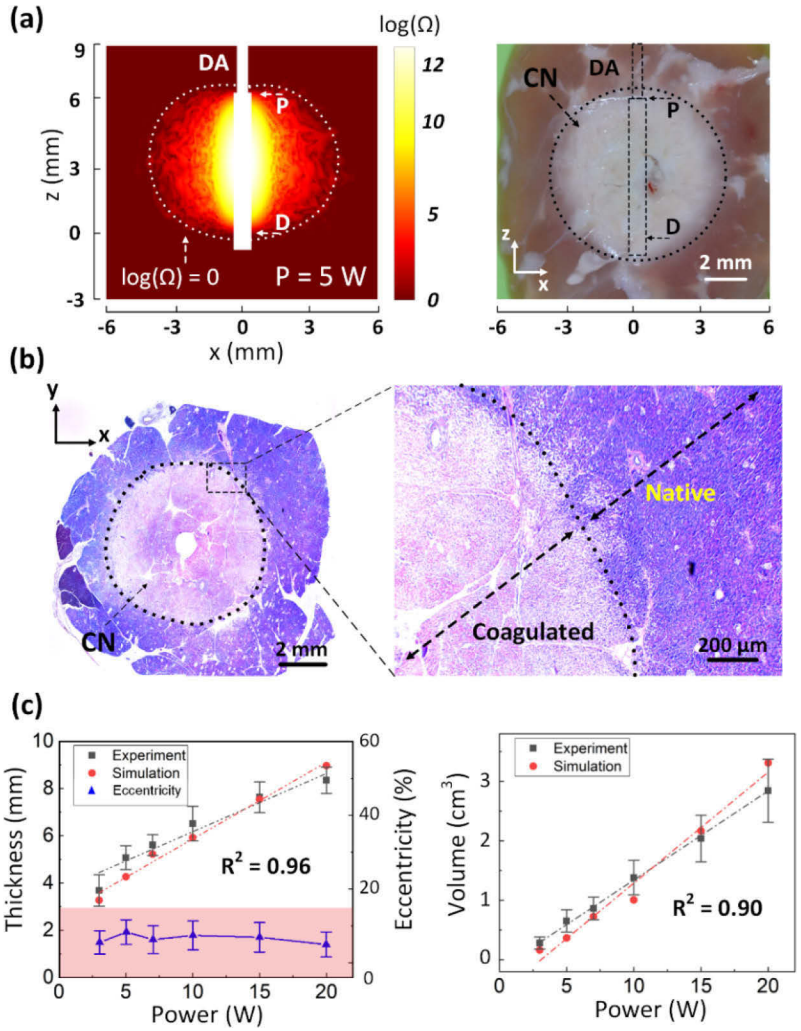

Fig. 5. Assessments of irreversible thermal ablation in *ex vivo* pancreatic tissue after 5-W CILA: (a) numerical simulation (left) and experiment (right) on irreversible tissue ablation after irradiation of 5 W for 200 s (1000 J delivered; DA = diffusing applicator; CN = coagulation necrosis), (b) histology images of transverse section (xy plane) from tissue treated at 5 W for 200 s (left: 40× and right: 400×), and (c) radial thickness of tissue ablation and eccentricity (left) and total ablation volume (right) as function of power (N = 10).

Biomedical Optics EXPRESS

was comparable with those from both numerical simulation and *ex vivo* tests ($p = 0.48$; left in Fig. 6(c)). The estimated eccentricity of the *in vivo* results was still less than 15% (red area; left in Fig. 6(c)), indicating that the EUS-guided CILA uniformly generated a circular area of coagulation necrosis around the diffusing applicator in the tissue. Ablation volume was also comparable between the *ex vivo* (0.65 ± 0.19 cm^3) and *in vivo* (0.71 ± 0.23 cm^3) tests ($p = 0.43$; right in Fig. 6(c)). It was noted that the *in vivo* ablation volume was slightly larger than that of the *ex vivo* due to the difference in the initial temperature. Table 3 compares ablation performance of CILA from numerical simulations, *ex vivo*, and *in vivo* tests.

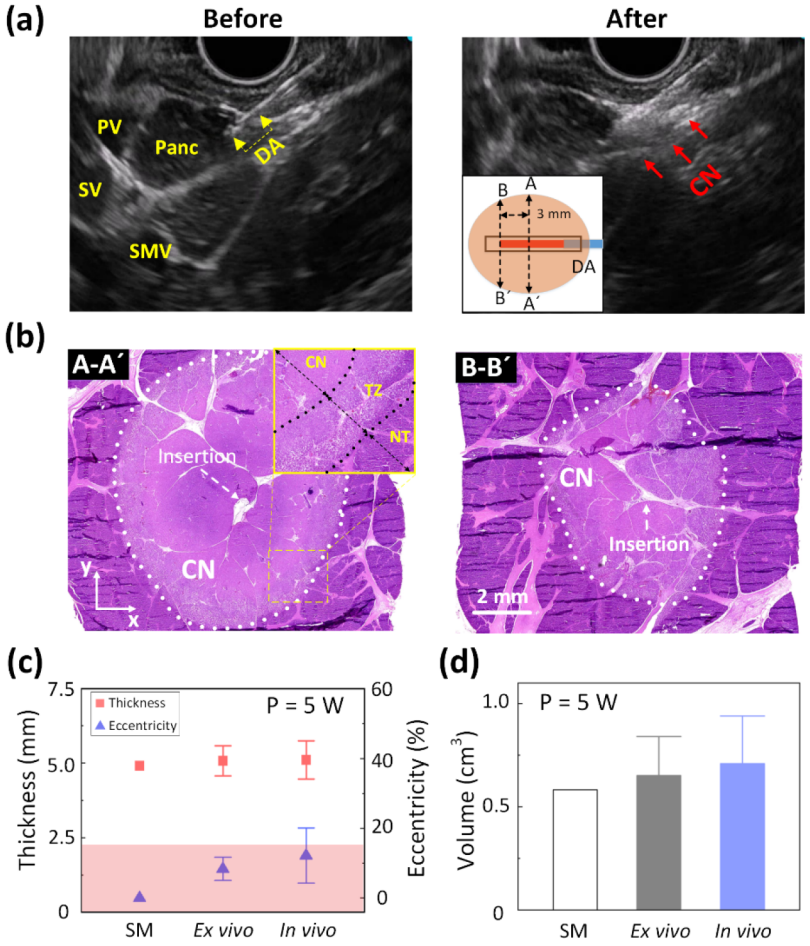

Fig. 6. EUS-guided CILA on pancreatic tissue in *in vivo* porcine models (5 W for 200 s; 1000 J delivered): (a) US images captured before (left) and after (right) CILA (DA = diffusing applicator; PV = Portal vein; SV = Splenic vein; SMV = Superior mesenteric vein; Panc = Pancreas; CN = coagulation necrosis), (b) histology images (40×) of transverse tissue sections (xy plane) from A-Á(middle of DA; left) and B-B´ (3 mm away from distal end of DA; right), and (c) quantitative comparisons of ablation thickness and eccentricity (left) and ablation volume (right) among simulation (SM), *ex vivo* tests (N = 10), and *in vivo* tests (N = 2), and radiofrequency ablation (RFA). An inlet in (a) illustrates coagulation necrosis around DA in the tissue. An inlet in (b) presents microscopic changes in the ablated tissue (100×; TZ = transition zone; NT = native tissue).

Biomedical Optics EXPRESS

Table 3. Comparison of ablation performance of CILA (5 W for 200 s; energy delivery = 1000 J)

Group	N	Ablation thickness (mm) [range]	Ablation volume (cm^3) [range]
Simulation	-	4.9	0.58
Ex vivo	10	5.1 ± 0.5 [4.6~5.7]	0.65 ± 0.19 [0.48~0.91]
In vivo	2	5.2 ± 0.7 [4.6~5.6]	0.71 ± 0.23 [0.54~0.87]

4. Discussion

The current *ex vivo* study shows a linear relationship between the applied power and the extent of thermal damage (Fig. 5), which agrees well with the previous study [13]. Despite the delivery of the same total energy (1000 J), higher power levels rapidly increased surface and interstitial tissue temperatures as the volumetric heat deposition was faster than conductive heat diffusion to the surrounding tissue. A flat fiber used for the previous study yielded less predictable ablation size because of the nonlinear effects from tissue carbonization during treatment [13]. The carbonization accumulated at the fiber tip because the tissue adhesion lowers light transmission and eventually degrades the fiber tip. Matteo *et al.* reported that ablation volume became saturated at 10 W as carbonization volume significantly increased. The ramification of the carbonization in clinical situations indicates ILA-associated complications, such as an excessive extent of thermal injury at a given energy, an unpredictable thermal lesion, potential perforation, and delayed wound healing. Conversely, a diffusing applicator has an irradiance of 45 W/cm^2 at 5 W, which is 150-fold lower than that of the flat fiber (7000 W/cm^2 at 5 W). In turn, the diffusing applicator distributes optical energy widely along the diffusing tip in a cylindrical manner and prevents the rapid accumulation of thermal energy in the tissue and the occurrence of tissue carbonization, unlike the flat fiber. Thus, CILA was able to create predictable and uniform ablation in the ex vivo and in vivo pancreatic tissue. In addition, it was observed that the diffusing applicator was inserted through a 19-G needle under EUS-guidance on two mini-pigs without physical damage (Fig. 6). Hence, the EUS-guided CILA, with enhanced safety from the diffusing applicator, may avoid the complications associated with insertion/bending damage or tissue carbonization during PC treatments.

Clinical situations may require multiple, consecutive ILAs to cover a large-sized tumor for sufficient treatment. A minimum number of fiber insertions is often conducive to PC treatment to reduce complications and procedural complexity. CILA with 1064 nm light can be more beneficial for minimally invasive treatment of PC because of the shorter irradiation time (few minutes), deep thermal penetration (i.e., ≥ 4 mm), larger ablation volume, and less heat-sink effects, compared to RFA [13, 27, 28]. Moreover, CILA demonstrated a therapeutic capacity of abating the pancreatic tissue in a wide range of ablation volumes (0.28–2.84 cm^3; Table 2), which is larger than that of RFA (0.24 ± 0.08 cm^3) [11]. Therefore, multiple CILAs with augmented thermal effects and minimal fiber degradation can contribute to minimal tissue insertions and effective treatment of large-sized PC in clinical situations.

The extent of thermal ablation accompanied hyperechoic changes in transverse US images around the diffusing tip during laser irradiation (Fig. 4(c) and Fig. 6(a)), which was also reported in the previous study [13]. As tissue temperature increases up to 60 °C, the onset of coagulation necrosis accompanies micro-bubbles as well as changes in tissue elasticity [29, 30]. Thus, the increased echogenicity affects the posterior acoustic shadow during US imaging, indicating irreversible thermal responses of the tissue to the laser irradiation. The proposed CILA is well compatible with US and EUS guidance to position the diffusing tip and to monitor the on-going treatment size visually without adverse effects. Although EUS has clinically been used as a visual guidance, high sensitivity of the pancreas to temperature requires precise temperature control during the procedure. Moreover, Park *et al.* (2019) and Zhou *et al.* (2019) suggested

Biomedical Optics EXPRESS

that ultrasound thermal imaging can assist thermal dosage evaluations by measuring the changes in tissue elasticity of a lesion and monitoring spatial temperature distributions during RFA and laser ablation, respectively [29, 30]. Therefore, in order to warrant clinical safety, CILA can be evaluated with various monitoring techniques, such as ultrasound thermal imaging and fiber radiometric thermometer to further monitor the temperature development and the extent of coagulation lesion, eventually enhancing the treatment accuracy as well as safety during the procedure [29–32]. In addition, an EUS-guided CILA in conjunction with color Doppler analysis will increase the accuracy of ablation monitoring and prevent unwanted injury to blood vessels and peripheral tissue structures during PC treatment.

Although the current study showed the clinical feasibility of EUS-guide CILA for treating pancreatic tissue, experimental limitations remain. Both numerical and experimental results showed good agreement in ablation volumes for both *ex vivo* and *in vivo* tests. However, normal porcine pancreatic tissue hardly reflects the pathological features of human PC, especially pancreatic tumor. In fact, absorption/scattering coefficients and anisotropy factor can be changed as native tissue becomes fully coagulated during thermotherapy [33]. However, no optical properties for the coagulated pancreatic tissue are available in the published literature. Therefore, further studies should be performed to measure the dynamic variations in the optical properties of the pancreatic tissue during 1064-nm CILA. Thus, the numerical simulations with the temperature-dependent physical properties of the pancreatic tissue can determine treatment dosage for CILA with accuracy and predict the corresponding ablation volume for clinical translation. In spite of the success in the *in vivo* EUS-guided CILA, the number of mini-pigs was relatively small (N=2), and one power level (5 W) was merely employed for the current study. In fact, higher power levels (7 or 10 W) can be applied to improve the efficacy of CILA as long as ablation time can be controlled. Thus, further investigations with a larger number of mini-pig models will be necessary to identify the optimal laser condition for CILA as well as acute and chronic responses of the treated tissue. Additionally, the effect of laser light on major blood vessels and biliary duct should be evaluated to warrant the safety of the EUS-guided CILA prior to clinical application. While the current study used a 19-G needle to insert a diffusing applicator into pancreatic tissue, clinical translation of the proposed CILA may require a smaller diameter of needle (22-G) for reducing mechanical trauma. Fabrication of a smaller diffusing applicator (core size = 200 μm) will be required to comply with the 22-G needle. Future studies will examine the performance of the smaller diffusing applicator with an EUS endoscope in terms of mechanical and structural integrity, flexible insertion, and fiber degradation during the EUS-guided CILA.

5. Conclusion

A diffusing applicator with a cylindrical light distribution created a predictable and uniform ablation volume in *ex vivo* and *in vivo* pancreatic tissue without carbonization. The current findings suggest a therapeutic capacity of EUS-guided CILA to treat unresectable PC with enhanced safety and no technical difficulties. Further *in vivo* investigations are expected to warrant efficacy and safety of the proposed EUS-guided CILA in a clinical setting.

Funding. The Korea government (the Ministry of Science and ICT, the Ministry of Trade, Industry and Energy, the Ministry of Health & Welfare, the Ministry of Food and Drug Safety) (202016B01); The National Research Foundation of Korea (the Ministry of Education) (2021R1A6A1A03039211).

Acknowledgments. This work was supported by the Korea Medical Device Development Fund grant funded by the Korea government (the Ministry of Science and ICT, the Ministry of Trade, Industry and Energy, the Ministry of Health & Welfare, the Ministry of Food and Drug Safety) (Project Number: 202016B01) and Basic Science Research Program through the National Research Foundation of Korea (NRF) funded by the Ministry of Education (No. 2021R1A6A1A03039211). We would like to thank Dr. Kathy Wiemers for her professional language editing and valuable advice.

Disclosures. The authors declare that there are no conflicts of interest related to this article.

Biomedical Optics EXPRESS

Data availability. Data underlying the results presented in this paper are not publicly available at this time but may be obtained from the authors upon reasonable request.

References

1. F. Bray, J. Ferlay, I. Soerjomataram, R. L. Siegel, L. A. Torre, and A. Jemal, "Global cancer statistics 2018: GLOBOCAN estimates of incidence and mortality worldwide for 36 cancers in 185 countries," Ca-Cancer J. Clin. **68**(6), 394–424 (2018).
2. A. Bengtsson, R. Andersson, and D. Ansari, "The actual 5-year survivors of pancreatic ductal adenocarcinoma based on real-world data," Sci. Rep. **10**(1), 1–9 (2020).
3. J. M. DeWitt, K. Sandrasegaran, B. O'Neil, M. G. House, N. J. Zyromski, A. Sehdev, S. M. Perkins, J. Flynn, L. McCranor, and S. Shahda, "Phase 1 study of EUS-guided photodynamic therapy for locally advanced pancreatic cancer," Gastrointestinal Endoscopy **89**(2), 390–398 (2019).
4. S. Lakhtakia, M. Ramchandani, D. Galasso, R. Gupta, S. Venugopal, R. Kalpala, and D. N. Reddy, "EUS-guided radiofrequency ablation for management of pancreatic insulinoma by using a novel needle electrode (with videos)," Gastrointestinal Endoscopy **83**(1), 234–239 (2016).
5. T. J. Song, D. W. Seo, S. Lakhtakia, N. Reddy, D. W. Oh, D. H. Park, S. S. Lee, S. K. Lee, and M.-H. Kim, "Initial experience of EUS-guided radiofrequency ablation of unresectable pancreatic cancer," Gastrointestinal Endoscopy **83**(2), 440–443 (2016).
6. F. M. Di Matteo, P. Saccomandi, M. Martino, M. Pandolfi, M. Pizzicannella, V. Balassone, E. Schena, C. M. Pacella, S. Silvestri, and G. Costamagna, "Feasibility of EUS-guided Nd: YAG laser ablation of unresectable pancreatic adenocarcinoma," Gastrointestinal Endoscopy **88**, 168–174 e161 (2018).
7. H. Strunk, J. Henseler, M. Rauch, M. Mücke, G. Kukuk, H. Cuhls, L. Radbruch, L. Zhang, H. Schild, and M. Marinova, "Clinical use of high-intensity focused ultrasound (HIFU) for tumor and pain reduction in advanced pancreatic cancer," Röfo. **188**(7), 662–670 (2016.
8. S. E. Jung, S. H. Cho, J. H. Jang, and J.-Y. Han, "High-intensity focused ultrasound ablation in hepatic and pancreatic cancer: complications," Abdominal imaging **36**(2), 185–195 (2011).
9. P. Saccomandi, A. Lapergola, F. Longo, E. Schena, and G. Quero, "Thermal ablation of pancreatic cancer: a systematic literature review of clinical practice and pre-clinical studies," Int. J. Hyperthermia **35**(1), 398–418 (2018).
10. M. G. Keane, K. Bramis, S. P. Pereira, and G. K. Fusai, "Systematic review of novel ablative methods in locally advanced pancreatic cancer," World journal of gastroenterology: WJG **20**(9), 2267 (2014).
11. M. Barret, S. Leblanc, A. Rouquette, S. Chaussade, B. Terris, and F. Prat, "EUS-guided pancreatic radiofrequency ablation: preclinical comparison of two currently available devices in a pig model," Endosc. Int. Open. **7**, E138–E143 (2019).
12. F. Di Matteo, M. Martino, R. Rea, M. Pandolfi, C. Rabitti, G. M. P. Masselli, S. Silvestri, C. M. Pacella, E. Papini, and F. Panzera, "EUS-guided Nd: YAG laser ablation of normal pancreatic tissue: a pilot study in a pig model," Gastrointestinal Endoscopy **72**(2), 358–363 (2010).
13. F. Di Matteo, M. Martino, R. Rea, M. Pandolfi, F. Panzera, E. Stigliano, E. Schena, P. Saccomandi, S. Silvestri, and C. M. Pacella, "US-guided application of Nd: YAG laser in porcine pancreatic tissue: an ex vivo study and numerical simulation," Gastrointestinal Endoscopy **78**(5), 750–755 (2013).
14. P. Saccomandi, E. Schena, M. A. Caponero, F. M. Di Matteo, M. Martino, M. Pandolfi, and S. Silvestri, "Theoretical analysis and experimental evaluation of laser-induced interstitial thermotherapy in ex vivo porcine pancreas," IEEE Trans. Biomed. Eng. **59**(10), 2958–2964 (2012).
15. A. Johansson, F. Faber, G. Kniebühler, H. Stepp, R. Sroka, R. Egensperger, W. Beyer, and F. W. Kreth, "Protoporphyrin IX fluorescence and photobleaching during interstitial photodynamic therapy of malignant gliomas for early treatment prognosis," Lasers Surg. Med. **45**(4), 225–234 (2013).
16. S. Van Esser, G. Stapper, P. Van Diest, M. van den Bosch, J. Klaessens, W. T. M. Mali, I. B. Rinkes, and R. Van Hillegersberg, "Ultrasound-guided laser-induced thermal therapy for small palpable invasive breast carcinomas: a feasibility study," Annals of Surgical Oncology **16**(8), 2259–2263 (2009).
17. E. Rohde, I. Mesecke-von Rheinbaben, A. Roggan, H. Podbielska, M. Hopf, and G. Müller, "Interstitial laser-induced thermotherapy (LITT): comparison of in-vitro irradiation effects of Nd: YAG (1064 nm) and diode (940 nm) laser," Medical Laser Application **16**(2), 81–90 (2001).
18. V. N. Tran, H. S. Lee, V. G. Truong, Y. H. Rhee, and H. W. Kang, "Concentric photothermal coagulation with basket-integrated optical device for treatment of tracheal stenosis," Journal of Biophotonics **11**(1), e201700073 (2018).
19. V. G. Truong, J. Hwang, and H. W. Kang, "Effect of spatial light distribution on the thermal response of vascular tissue," Biomed. Opt. Express **9**(7), 3037–3048 (2018).
20. V. G. Truong, S. Park, and H. W. Kang, "Spatial effect of conical angle on optical-thermal distribution for circumferential photocoagulation," Biomed. Opt. Express **8**(12), 5663–5674 (2017).
21. A. J. Welch and M. J. Van Gemert, *Optical-thermal Response of Laser-irradiated Tissue* (Springer, 2011).
22. D. Yang, M. C. Converse, D. M. Mahvi, and J. G. Webster, "Expanding the bioheat equation to include tissue internal water evaporation during heating," IEEE Trans. Biomed. Eng. **54**(8), 1382–1388 (2007).
23. A. McKenzie, "Physics of thermal processes in laser-tissue interaction," Phys. Med. Biol. **35**(9), 1175–1209 (1990).

Biomedical Optics EXPRESS

24. A. Paul, A. Narasimhan, F. J. Kahlen, and S. K. Das, "Temperature evolution in tissues embedded with large blood vessels during photo-thermal heating," J. Therm. Biol. **41**, 77–87 (2014).
25. P. Saccomandi, E. S. Larocca, V. Rendina, E. Schena, R. D'Ambrosio, A. Crescenzi, F. M. Di Matteo, and S. Silvestri, "Estimation of optical properties of neuroendocrine pancreas tumor with double-integrating-sphere system and inverse Monte Carlo model," Lasers in Medical Science **31**(6), 1041–1050 (2016).
26. M. S. Adams, S. J. Scott, V. A. Salgaonkar, G. Sommer, and C. J. Diederich, "Thermal therapy of pancreatic tumours using endoluminal ultrasound: parametric and patient-specific modelling," Int. J. Hyperthermia **32**(2), 97–111 (2016).
27. T. Ishikawa, M. Zeniya, K. Fujise, A. Hokari, and G. Toda, "Clinical application of Nd: YAG laser for the treatment of small hepatocellular carcinoma with new shaped laser probe," Lasers Surg. Med. **35**(2), 135–139 (2004).
28. A. A. Meesters, L. H. Pitassi, V. Campos, A. Wolkerstorfer, and C. C. Dierickx, "Transcutaneous laser treatment of leg veins," Lasers in Medical Science **29**(2), 481–492 (2014).
29. S. Park, J. Hwang, J. E. Park, Y. C. Ahn, and H. W. Kang, "Application of ultrasound thermal imaging for monitoring laser ablation in ex vivo cardiac tissue," *Lasers Surg. Med.* (2019).
30. Z. Zhou, Y. Wang, S. Song, W. Wu, S. Wu, and P.-H. Tsui, "Monitoring microwave ablation using ultrasound echo decorrelation imaging: an ex vivo study," Sensors **19**(4), 977 (2019).
31. Y.-D. Liu, Q. Li, Z. Zhou, Y.-W. Yeah, C.-C. Chang, C.-Y. Lee, and P.-H. Tsui, "Adaptive ultrasound temperature imaging for monitoring radiofrequency ablation," PloS one **12**, e0182457 (2017).
32. P. L. Franz and H. Wang, "Development of hyperthermia measurable fiber radiometric thermometer for thermotherapy," J. Biophotonics **13**, e201960205 (2020).
33. J. P. Ritz, A. Roggan, C. Isbert, G. Müller, H. J. Buhr, and C. T. Germer, "Optical properties of native and coagulated porcine liver tissue between 400 and 2400 nm," Lasers Surg. Med. **29**(1), 205–212 (2001).